

In-field phasing at the upgraded GMRT

Sanjay Kudale¹, Jayanta Roy¹, Jayaram N. Chengalur^{1,2},
Shyam Sharma¹, Sangita Kumari¹

ABSTRACT

In time-domain radio astronomy with arrays, voltages from individual antennas are added together with proper delay and fringe correction to form the beam in real-time. In order to achieve the correct phased addition of antenna voltages one has to also correct for the ionospheric and instrumental gains. Conventionally this is done using observations of a calibrator source located near to the target field. This scheme is sub-optimal since it does not correct for the variation of the gains with time and position in the sky. Further, since the ionospheric phase variation is typically most rapid at the longest baselines, the most distant antennas are often excluded while forming the beam. We present here a different methodology ("in-field phasing"), in which the gains are obtained in real-time using a model of the intensity distribution in the target field, which overcomes all of these drawbacks. We present observations with the upgraded Giant Metre-wave Radio Telescope (uGMRT) which demonstrates that in-field phasing does lead to a significant improvement in sensitivity. We also show, using observations of the millisecond pulsar J1120–3618 that this in turn leads to a significant improvement of measurements of the Dispersion Measure and Time of Arrival. Finally, we present test observations of the GMRT discovered eclipsing black widow pulsar J1544+4937 showing that in-field phasing leads to improvement in the measurement of the cut-off frequency of the eclipse.

Subject headings: pulsars: general; binaries: eclipsing, pulsars: individual, pulsar: phased array Calibration, pulsar:real-time calibration

¹National Centre for Radio Astrophysics, Pune 411 007, India

²Tata Institute of Fundamental Research, Mumbai 400 005, India

1. Introduction

In radio astronomy calibration to correct for instrumental and ionospheric perturbations to the amplitude and phase of the received astrophysical signal is essential. In particular, at low radio frequencies, it is important to calibrate the ionospheric phases quite frequently. This is typically done by interleaving observations of a nearby (i.e. to the target field) calibrator source with the target field observation. In post-processing, these calibrator observations are used to interpolate the phase corrections which are then applied to the data. For time domain astronomy typically a high-time resolution data stream is provided by combining the voltages of the antennas in the array in real time to produce a "phased array" or "tied array" beam. Conventionally, for such observations, a nearby calibrator is observed just prior to the target observations in order to "phase up" the array. This scheme suffers from a number of drawbacks. Firstly, it does not allow for correction of the variation of the phases with time and position in the sky. Secondly, since the ionospheric phase varies most rapidly on the longest baselines, typically the most distant antennas are excluded while forming the beam. All of this leads to a significant loss in sensitivity. Finally, this external calibration needs to be done quite frequently, typically once in 30-40 minutes. This not only leads to increased observation overheads (about 15-20%), but also makes it not possible to have long uninterrupted observations of the target source. This can be a limiting factor for some studies, e.g. observations of binary and eclipsing pulsars for scanning full orbital phase (typically few hours long), repeating Fast Radio Bursts (FRBs), faint pulsars which need few hours of phase coherent folding for detection, intermittent pulsars etc.

For imaging observations, it has long been the practice to iteratively improve the dynamic range of the image by estimating antenna based gains from the target observations themselves, a process known as "self-calibration" (Cornwell et al., (1999), Thompson A. R., et al., (2017)). Here we present a real time implementation of this at the upgraded GMRT (uGMRT, (Gupta et al., 2017)) where a pre-existing model of the target field is used to determine and apply the phases while forming the phased array beam. We also present observations comparing in-field calibration with conventional calibration, which shows that in-field calibration does indeed lead to significant improvement in the sensitivity, which in turn leads to improvements in measurements of the Dispersion Measure (DM), Time of Arrival (TOA), as well as the cut-off frequency of the eclipse for eclipsing pulsars.

The rest of the paper is organized as follows. We describe the methodology in section 2. The Observation and analysis details are presented in section 3. In section 4 we present observations taken to validate the in-field phasing implementation, as well as to compare it with conventional phasing. Observations of two GMRT discovered millisecond pulsars (MSPs) are presented in section 4.1, allowing a translation of the improvement in the sensi-

tivity into increased accuracy of parameters of interest such as the DM, TOA, eclipse cut-off frequency etc. We summarise the results in section 5.

2. Methodology

Radio telescope arrays measure *visibilities*, i.e. the pairwise cross-correlation between the signals from all antennas. In the absence of baseline based errors and non-isoplanatic effects, the observed visibilities V_{ij} can be written as in equation 1, where \widehat{V}_{ij} are true visibilities, g_i are antenna based complex gains and η_{ij} is the noise. Note that the gain includes both instrumental as well as ionospheric contributions.

$$V_{ij}(t) = g_i(t)g_j^*(t)\widehat{V}_{ij}(t) + \eta_{ij}(t) \quad (1)$$

If the true visibilities \widehat{V}_{ij} are known, then this equation can be used to estimate the antenna based gains by minimizing

$$L = \sum_{i=1}^N \sum_{j=i+1}^N w_{ij} |V_{ij} - g_i g_j^* \widehat{V}_{ij}|^2 \quad (2)$$

where w_{ij} are suitable weights. In the most straight forward case, observations of a known isolated point source (i.e. for which \widehat{V}_{ij} is a constant) can be used for solving for the antenna gains. If one assumes that the gains vary only slowly with time and position in the sky, these solutions can also be used to calibrate the target visibilities. However, as is well known, for an N element array the number of complex unknowns in Eqn. 2 is much smaller than the number of measurements ($\sim N^2$), and schemes to iteratively solve for both the true visibilities as well as the unknown complex gains (i.e. self-calibration, Cornwell et al., (1999)) converge rapidly. As such Eqn. 2 can be used to determine the gain for quite complex fields, even if one starts with a relatively crude initial estimate of the gains. In situations where the true visibilities are already known (for e.g. from an earlier observation), Eqn. 2 can be used to directly estimate the antenna based gains without the need for observations of a standard calibrator source. In particular, for phased array observations of a field in which the true visibilities are known Eqn. 2 can be used not just to directly phase the array (thus eliminating the error introduced by the ionospheric phase difference between the target and calibrator source directions), but also to correct for any time variability since the gains can be updated in quasi real time.

Kudale & Chengalur, (2017) had presented an implementation of this scheme for the legacy GMRT correlator, i.e. the GMRT Software Back-end (GSB, Roy, J et al., (2010)). The

GSB had a bandwidth of 33 MHz band-width divided into a maximum of 512 channels. The implementation used the *flagcal* package (Prasad & Chengalur, (2012), Chengalur, (2013)) to flag the data and determine the antenna based gains for individual channels by using direct Fourier transform (DFT). The upgrade of the GMRT (Gupta et al., (2017) replaced the GSB with the GMRT Wide-Band backend (GWB, Reddy et al., (2017)), which allows for up to 16384 spectral channels with a total bandwidth of up to 400 MHz. The DFT implementation in *flagcal* is sub-optimal for real-time applications, and hence an FFT-based solver was added to the package. All the observations presented here use this updated solver.

For wide fields of view, accurate calculation of the model visibilities requires one to account for non-coplanarity of the baselines (the so called "w" correction, see e.g. Cornwell et al., (2008). This is computationally expensive, and is not part of the current implementation. To estimate the magnitude of the error introduced, we tested out the solver on simulated fields with a single strong point source (~ 1 Jy) situated at a range of distances from the phase centre of the field. We find that if the source lies within $\sim 20'$ from phase center at band-4 (550–750 MHz) and within $\sim 30'$ from phase center at band-3 (300–500 MHz), the rms phase errors are less than $\sim 5^\circ$, which is small compared to the noise. All of the observations presented here are for fields where there are no dominant sources lying beyond the above limits. The 'w' correction would be important for sources with dominant sources at the edge of the field of view. Correction for the 'w' term is more computationally expensive and is deferred to a later implementation.

3. Observation and analysis

A number of test observations were carried out to compare the performance of in-field phasing with that of conventional phasing. Specifically we observed the normal pulsar B0740–28 in the GMRT Band 4(550–750 MHz) and two millisecond pulsars J1120–3618 and J1544+4937 in the GMRT Band 3 (300–500 MHz), all with 200 MHz bandwidth. J1120–3618 is one of the fainter MSP discovered with GMRT (Bhattacharyya et al., (2022) while MSP J1544+4937 is an eclipsing binary pulsar (Bhattacharyya et al., (2013)). Eclipsing binaries are a special class of fast-spinning MSPs in compact binary systems, where the companions are ablated away by energetic pulsar winds with ablated material from the companion overflowing companion's Roche lobe (e.g. Roberts, (2012)). The intra-binary material can obscure the pulsar's emission for part of its orbit, resulting in eclipses. A black widow is a subclass of eclipsing binaries characterised by a very low companion mass (M_c), i.e. $M_c < 0.1 M_\odot$.

In order to facilitate the comparison, the observations were carried out in two modes:

conventional phasing using an external calibrator source and in-field phasing. For the conventional phasing we observed the calibrator 0837–198 for B0740–28, 1154–35 for J1120–3618, and 1459+716 for J1544+4937. The conventional phasing was done only once, at the start of the observation. For the in-field phasing we used a sky-model for these fields obtained from earlier observations. The model visibilities obtained from this sky model, along with the real-time visibilities measured by the GWB were used to solve for per antenna phases in real-time. These phase corrections were applied to the output of FFT inside the GWB. The software allows for the phases to be updated without needing a break in the observations.

The GWB allows for the formation of up to 4 beams along with the visibility data. For our observations we typically used three beams. The antennas whose data is to be combined can be chosen independently for each beam. The GMRT has a hybrid configuration with about half the antennas in a central compact configuration and the remaining in 3 roughly "Y" shaped arms. The first beam ("beam1") typically used antennas from the compact array and the 1st arm antenna, while the third beam ("beam3") used all the antennas, i.e. including the extreme arm antennas. The second beam ("beam2") was intermediate between these two, typically including up to the 3rd arm antenna. The actual antennas used to form each beam varied from run to run, depending on the antennas that were available for use at the given time. But overall "beam1" was restricted to relatively short baselines, "beam3" included the longest available baselines, while "beam2" is intermediate between these two. Note also that all the antennas used for producing "beam1" were also included for producing "beam2". Similarly all the antennas used for producing "beam2" are also included for producing "beam3". Finally we note in passing that since tied arrays are formed by adding the phased voltages and squaring their output also contains a contribution from the auto-correlations of the individual antennas (i.e. the "incoherent array" output), which is independent of the phase errors (see e.g. Roy, J. et al., (2018)).

The results presented next for the beam data were obtained via analysis using *SIGPROC* (Lorimer D. R., (2011)) and *PRESTO* (Scott Ransom et al., (2002)) for folding and *TEMPO2* (Hobbs G. et al., (2006)) for timing analysis.

4. Results

The first set of results we obtained were from observations aimed at testing the in-field observing mode and optimising the observation strategy. We examine the variation of the SNR (signal-to-noise ratio) with time and finalize a strategy which keeps the SNR constant, as expected for in-field phasing. In the second set of observations, we use the updated observation strategy to demonstrate the scope of in-field phasing to enhance the scientific

output of the GMRT for time-domain science.

4.1. Testing the in-field phasing scheme

For probing the phasing effectiveness with in-field phasing we carried out observations on pulsar B0740–28 while simultaneously recording data from three beams (i.e. beam1, beam2 and beam3) with an increasing number of antennas, as described above. At the start of the observation the array was phased using in-field phasing and for the remaining part, the pulsar data were recorded with scans of 5 minutes each for a duration of ~ 2.5 hours without any re-phasing. The pulsar SNR was computed for each scan, and the variation of SNR with scan number is shown in Fig. 1. As can be seen, beam1 (containing only short baselines) shows no drop in SNR (see the red curve in Part (a) of Fig. 1). In contrast, beam2 (which includes antennas at intermediate distances) shows an SNR drop up to $\sim 41\%$ of its starting SNR (see the green curve in Part (a) of Fig. 1), while beam3, which includes the longest available baselines, showed an SNR drop to $\sim 12\%$ of its starting SNR. (see the blue curve in Part (a) of Fig. 1). The figure also shows the fastest drop in SNR happens for beam3, in line with the expectation that phase variations are faster on the longer baselines. In passing we note that changes in ionospheric conditions over the array would lead to both a shift in the apparent position of the target pulsar (arising from any systematic gradients in the density) as well as a loss in sensitivity due to dephasing of the array (see e.g. Kudale & Chengalur, (2017)). Both of these effects will lead to an increasing loss of sensitivity for arrays that have a longer baselines.

Figure 1(b) shows another set of observations of the pulsar B0740–28. For the observations shown in the Part I (light red shaded region) the array was phased (using in-field phasing) only once at the start of the ~ 1.3 hour observation. On the other hand, for the observations shown in the Part II (light blue shaded region) the array phases were updated every 4 minutes using the data acquired during the earlier ~ 4 minutes scan. As before the data was recorded for 3 arrays, and as can be seen without in-field phasing the SNR degrades rapidly, particularly for beam3, the array with the longest baselines. On the other hand, with in-field phasing the SNR is approximately constant, as expected. It is interesting to note that the variation of SNR with time in the case where no continuous phase correction is done is quite different for the two different observing runs separated by ~ 1.5 years shown in Figure 1. In the observations shown in Figure 1(a) the SNR even for the longest array reduces gradually over the ~ 150 minutes observation span, whereas for the observations shown in Panel (b) of the same figure the SNR drops very sharply in the first ~ 20 minutes. At low frequencies, where the ionosphere can sometimes be fairly dynamic, these observed

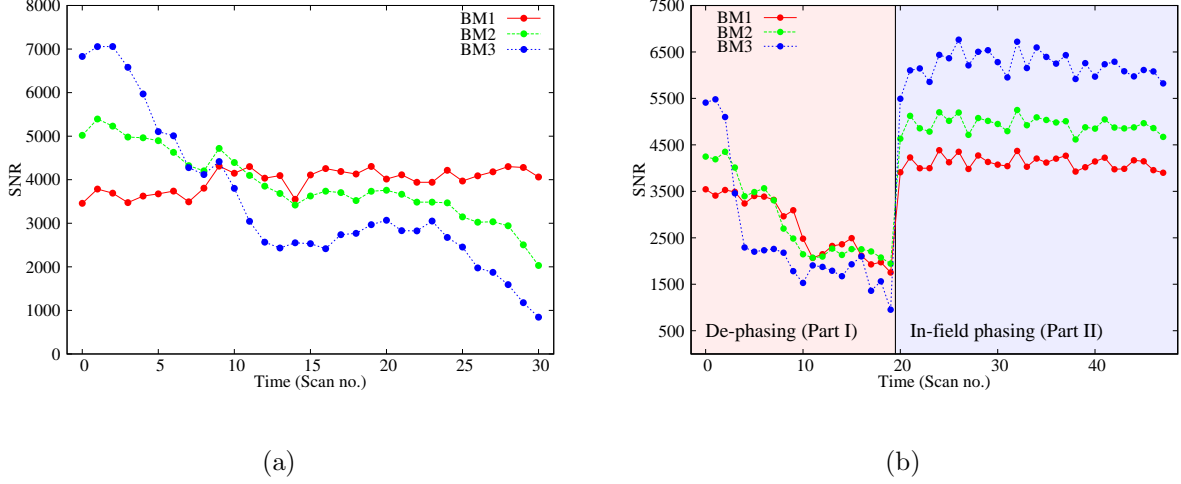


Fig. 1.— Part (a) : The drop in SNR for the different arrays as they de-phase with time. Phasing has been done only once at the start of the observation. The SNR is computed for scans ~ 5 minute duration. Part (b) : [Part I light red shaded region] The drop of SNR with time for different arrays as they de-phase with time. Phasing has been done only once at the start of the observations. Note that the SNR drop for this set of observations is much more rapid than for the observations shown in Part (a), showing the time variable characteristics of the de-phasing. [part II (light blue shaded region)] shows the SNR when in-field phasing carried out at regular intervals. The SNR is computed for scans of ~ 4 minute duration. In all panels larger array beam (beam3) is indicated by blue curve, moderate array size beam (beam2) is shown by green curve and smaller size array (beam1) is shown with red curve.

sharp drops in the SNR are indicative of the limitations of conventional phasing.

Figure 2 shows the SNR variation with conventional and in-field phasing for a weak millisecond pulsar MSP J1120–3618 (which was discovered at the GMRT, (Bhattacharyya et al., 2022)). The top panel shows the variation of SNR with time for a conventionally phased observation. The middle panel shows the variation of SNR for in-field phasing with a time interval of 4.5 minutes between successive phase updates, while the third panel shows the variation of SNR for in-field phasing for a time interval of 1.5 minutes between successive phase updates. All of these observations carried in close succession. As before data is shown for three different beams, with the same colour coding as for Figure 1. Please note that the time scale is different for the three different panels, with the top panel showing only 10 minutes of data. As can be seen, even over as short a time interval as 10 minutes, the SNR degrades quite significantly (to $\sim 50\%$ of its original value) in the case of conventional phasing. On the other hand, with in-field phasing the SNR does not show measurable degradation

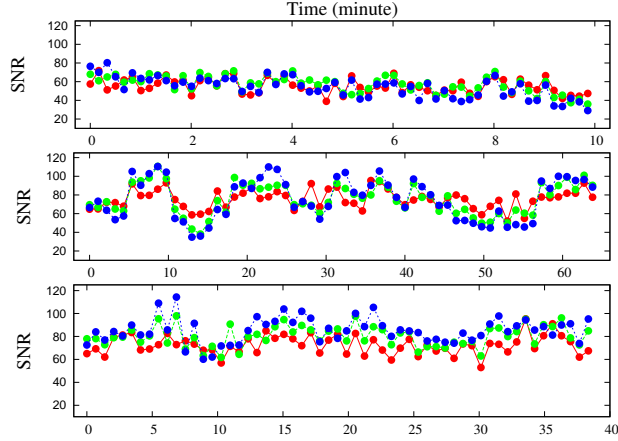


Fig. 2.— Sub-interval SNR variation over observation duration. Top panel showing SNR variation during observation with conventional phasing carried once in beginning. Middle panel shows variation in sub-interval SNR during observation in which in-field phasing was carried regularly in background with 4.5 minutes solution interval. Bottom panel shows variation in sub-interval SNR during observation with solution interval of 1.5 minutes. In all panels, the color coding is the same as in Figure 1

even over timescales ~ 1 hour. For the observations with phase updates every 4.5 minutes (middle panel) one can see one quite prominent modulations of the SNR, although there is no clear long-term trend. Such modulations were also seen in some other test observations carried out with 4.5 minutes phase updates. We conjecture that this may be due to the ionosphere varying faster than the 4.5 minutes. Subsequently, we tried the phase update interval to 1.5 minutes, which as can be seen from the bottom panel of the figure results in a more constant SNR. For all the observations presented later in the paper the update interval was kept at 1.5 minutes.

We present here results on the improvement that in-field phasing at the GMRT makes to two specific measurements of scientific interest, i.e. the accuracy with which pulsar timing can be done, as well as the difference that it makes to studies of eclipsing pulsars.

The stable clock-like properties of MSPs enables precise measurement of their rotational and orbital (if in binary) parameters through accurate measurement of the TOAs of pulses. For the same reasons, MSPs are also excellent probes of propagation imprints from interstellar medium (ISM) as well as detecting low-frequency gravitational waves (GWs) (e.g. Foster, R. S. and Cordes, J.M., (1990)). For pulsar signal processing a mean stable pulse profile

over the observing span is obtained by dedispersion and folding beam data with suitable model parameters (Lorimer, D. R., (2004)). The TOAs are determined by cross-correlation of the observed mean pulse profile of each epoch with a high SNR template profile which is obtained by adding profiles from many observations performed at the same frequency (e.g. Taylor, J. H., (1992)). The observed pulsar profile is a scaled and shifted version of template as described by equation 3 where τ signifies the shift in the measured profile, a is the scaling factor and N is the additive noise in the TOA measurement. The sensitivity of observation plays an important role in reducing the timing noise to obtain TOAs with improved uncertainties.

$$P(t) = a + bT(t - \tau) + N(t) \quad (3)$$

The uncertainty in the TOA is given by the equation, $\sigma_{TOA} = \frac{W}{SNR}$, where W is pulse width, and SNR is sensitivity of profile. We present below in-field measurements of TOAs with the GMRT and compare the accuracy of the measurements with what is typically obtained via conventional phasing.

The second measurement that we present is for an eclipsing millisecond pulsar. Millisecond binary pulsars are believed to be formed via recycling, a process in which the pulsar accretes mass from a companion star in binary, resulting in faster spin period via angular momentum transfer (see e.g. Bhattacharyya (1992)). In a compact binary system, the pulsar could also ablate mass from the companion via a powerful pulsar wind. This material can then obscure the pulsar emission causing eclipses (e.g Podsiadlowski P. (1991); van den Heuvel & J. van Paradijs, (1988); Phinney E. S., et al., (1988); Kluzniak W. et al., (1988)). In general, the eclipse duration is dependent on the observation frequency and is typically longer at lower frequencies and shorter at higher frequencies. In many cases, the pulsar is detected throughout the entire orbit at higher frequencies where it shows eclipses at lower frequencies (e.g. Bhattacharyya et al., (2013)). In order to understand eclipse mechanism, it is essential to precisely measure the frequency at which eclipse starts, i.e. the cut-off frequency. In addition, the pulse TOAs show an excess delay in pulse arrival time at the eclipse boundaries caused by the propagation of pulses through the eclipsing material spread beyond the Roche lobe (Eggleton, P. P., (1983)) of the companion star. This delay in TOAs arises from an excess DM_{ex} associated with material that the radio pulses encounter at the eclipse boundaries as given by eqn. 4, where t_{ex} is delay in timing residual, F is frequency of observation. In turn, DM_{ex} can be used to compute electron column density N_e of the eclipsing materials (Eqn 5), as well as to constrain the eclipse mechanism.

$$DM_{ex} (pc\ cm^{-3}) = 2.4 * 10^{-10} * t_{ex}(\mu s) * F(MHz)^2 \quad (4)$$

$$N_e(cm^{-2}) = 3 * 10^{18} * DM_{ex}(pc\ cm^{-3}) \quad (5)$$

We present here results for two binary pulsars MSP J1120–3618 and MSP J1544+4937. Both pulsars were discovered at the GMRT (Bhattacharyya et. al., 2022 and Bhattacharyya et. al., 2013 respectively) and have been the target of many follow up observations using conventional phasing with the uGMRT. This provides a good baseline for comparison between conventional and in-field phasing. Table 1 lists the observation details for all the pulsars used for in-field phasing demonstrations.

Table 1: Observation details and parameters for MSPs

Pulsar	Period	Dispersion measure	Flux density	Freq.	No. of epochs	Obs. Span
	mili-sec	pc cm^{-3}	mJy	MHz		days
B0740–28	166.8	73.7	130	600.0	2	NA
J1120–3618	5.6	45.1	1	400.0	20	400
J1544+4937	2.2	23.2	5.4	400.0	2	NA

MSP J1120–3618 was discovered in the Fermi-directed survey with the GMRT and has a spin period of 5.6 ms, DM of 45.1 pc cm^{-3} , binary period of 5.6 days, minimum companion mass of 0.18 M_{\odot} , and flux density of ~ 1 mJy at 400 MHz (Bhattacharyya et al., (2022)). Decade long timing measurements for this system were presented by Sharma et al., (2024) who detected a systematic increase of DM with time. We observed this MSP with in-field phasing at the GMRT band-3 (300-500 MHz) with 81.92 μs time resolution and 4096 spectral channels across 200 MHz bandwidth (i.e. 48.8 kHz frequency resolution). Both this data as well as the comparison conventional phasing data that we show were in-coherently dispersed.

4.1.1. MSP J1120–3618 : Improvement in timing precision

We show here continued timing of this pulsar, carried out over the last ~ 1.6 years using in-field phasing. As discussed earlier, in-field phasing is expected to provide superior SNR not just because of improved phasing but also because the entire array is used in the observations, where as conventional phased arrays at the GMRT typically exclude the extreme arm antennas (i.e. using only about 70% of the array). For ease of comparison all the data were scaled to a fiducial integration time of 30 minutes and a 100 MHz bandwidth. The Dispersion Measure was estimated from the time of arrivals obtained by dividing the 200 MHz bandwidth into 16 sub-bands and averaging full observation length in one sub-

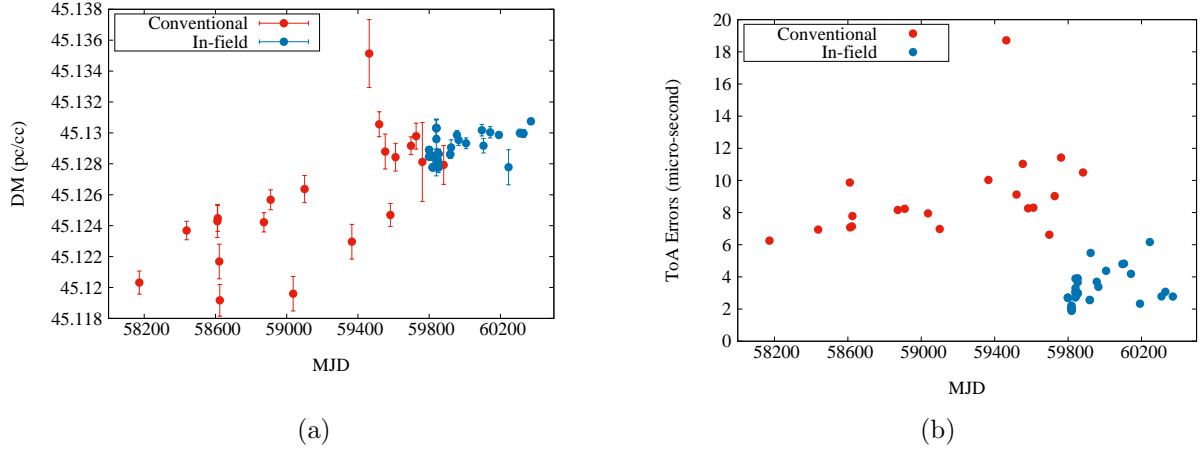


Fig. 3.— DM (Part (a)) and TOA errors (Part (b)) with conventional phasing observations (red points) and in-field phasing observations (blue points) for MSP J1120–3618.

integration. We carried PulsePortraiture-based wide-band timing analysis (Pennucci, T. T. et al., (2014), Sharma et al., (2022)) by modeling frequency-dependent effects and correcting for the evolution of the pulsar profile with frequency as carried in Sharma et al., (2024). We show in Fig. 3(a) the DM measurements obtained using in-field phasing (blue points); we achieve a median DM precision of $\sim 2.9 \times 10^{-4} \text{ pc cm}^{-3}$ which is about ~ 3 times better than that obtained via conventional phasing (i.e. $\sim 8.9 \times 10^{-4} \text{ pc cm}^{-3}$, red points). The TOA precision Fig. 3(b) also shown improvement by a factor of ~ 2.7 . The median TOA error for the in-field phasing (blue points) is $\sim 3 \mu\text{s}$, compared to $\sim 8.3 \mu\text{s}$ for conventional phasing (red points). The median SNR obtained from conventional phasing observations is ~ 56 and median SNR from in-field phasing observations is ~ 159 with their ratio of ~ 2.8 close to the improvement we achieved in DM and TOA precision.

4.1.2. MSP J1544+4937 : high time-frequency resolution probe for eclipse study

We carried observations of two consecutive eclipses i.e., separated by one full orbit. One eclipse was observed with conventional phasing and the following one was with in-field phasing, both having ~ 85 minutes of on-source time (spanning non-eclipsing orbital phases). We note that in the observations reported by Kumari et al., (2024) two consecutive eclipses separated by an orbit have shown different characteristics, viz change in eclipse cut-off frequency, excess N_e etc. The SNRs (scaled to 1 hour integration) of the pulse profile at the non-eclipsing phase are ~ 188 for the observation using conventional phasing and ~ 265

for the consecutive observation with in-field phasing.

We performed another observation of J1544+4937 with in-field phasing where we could probe the eclipse region in much more detail. We recorded phased array data with all the available antennas (22) at the time of the observation. These included the outer arm antennas. Using the best-fit parameters obtained by Kumari et al., (2023), we estimated the residuals across the eclipse (including some non-eclipsing orbital phases on either sides) region and derived the electron column density of the eclipsing materials N_e by using equation 5. The excess electron density derived from the TOAs are shown in Fig. 4. Kumari et al., (2023) had shown similar excess TOAs with a median time resolution of ~ 60 seconds. Given our higher sensitivity we measured the excess N_e at a range of time resolutions, viz. 93.9 seconds, 44.0 seconds and 5.5 seconds. As can be seen the higher time resolution observations show fine structure in the excess N_e , which is smoothed over at the coarser time resolution. This allows us to probe the variation of N_e across the eclipse and transitions in greater detail exploring the possible clumpy nature of eclipsing material around companion.

To obtain the eclipse cut-off frequency we followed the methodology described in Sharan et al., (2024, in preparation), in which data cube output of *PRESTO* (i.e. pulse intensity represented as function of sub-integration, sub-bands and phase bins) is analysed for eclipse duration. The finest frequency resolution (i.e. minimum number of sub-bands integration) of the data cube are checked for which pulse is detected above 5-sigma significance. We measured the eclipse cut-off frequency as 400 ± 1.6 MHz, which is a factor of ~ 3 times more precise than the measurements reported by Kansabanik et al., (2021) and Kumari et al., (2024)). However, we note that the 7 MHz error bars on cut-off frequency used in Kumari et al., (2024) was based on the requirement of allowing uniform resolution for all eclipses spanning over a longer duration. The individual eclipse boosted by scintillation can have better frequency resolution. This increased precision can be translated to more stringent limits on the physical parameters of the eclipse medium. We plan in our future paper to describe the quantitative estimation of eclipse parameters aided with in-field phasing sampling an ensemble of eclipses.

5. Summary

We present a scheme ("in-field phasing") for significantly improving the SNR of low frequency tied arrays where model visibilities of the target field are used to calibrate the array in quasi real time. This is expected to provide a number of improvements over conventional phasing where the array is periodically phased using observations of a calibrator near the target field. Conventional phasing does not correct for variations in the phase with time

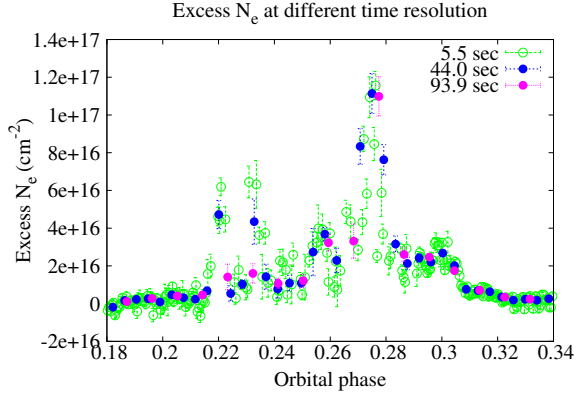


Fig. 4.— Measured excess electron column density for MSP J1544+4937 with in-field phasing for different time resolutions.

or position in the sky. Further, since the phase variation is typically most rapid on the distant baselines, for arrays like the GMRT, the most distant arm antennas are typically not used in tied arrays formed using conventional phasing. Finally since calibrator sources need to be periodically observed, conventional phasing does not allow for long contiguous observations of the target source. In-field phasing overcomes all of these drawbacks.

Using an implementation of in-field phasing at the upgraded GMRT (uGMRT) we show the improved performance of in-field phasing using observations of both normal as well as milli-second pulsars. For conventional phasing the signal to noise ratio (SNR) drops with time, with the SNR dropping further for arrays which include distant antennas, as expected. In contrast the SNR remains constant with time for in-field phasing, even for arrays that include the most distant arm antennas. For the uGMRT the use of in-field observations is shown to significantly increase the signal to noise ratio, even for relatively short (~ 1 hr) observations.

From observations of a milli-second pulsar (J1120–3618), we show that the improved SNR in in-field phasing translates to an improved precision in the measurement of the dispersion measure (DM), viz. a median DM precision of $\sim 2.9 \times 10^{-4} \text{ pc cm}^{-3}$, which is ~ 3 times better than the precision achieved using observations with conventional phasing. The median scaled TOA precision $\sim 3 \mu\text{s}$, also shows an improvement in precision by a factor ~ 3 . We also present observations of an eclipsing black-widow MSP J1544+4937 where in-field phasing allows for a more precise measurement of the eclipse cut-off frequency, as well as better measurements of the fine scale spatial structure of the eclipsing material as compared to earlier studies Kumari et al., (2024) and Kansabanik et al., (2021).

We acknowledge support of the Department of Atomic Energy, Government of India, under project no. 12-R&D-TFR-5.02-0700. The GMRT is run by the National Centre for Radio Astrophysics of the Tata Institute of Fundamental Research, India. We acknowledge support of GMRT telescope operators for observations.

REFERENCES

- A. Richard Thompson, James M. Moran, George W. Swenson Jr. Interferometry and synthesis in Radio Astronomy, A&A library, 2017
- Bhattacharyya, B., Roy, J., Ray, P. S., et al., 2013, ApJ Letters, 773, 12.
- Bhattacharyya, B., Roy, J., Freire, P. C. C., et al. 2022, ApJ, 933, 159
- Bhattacharya, D., ASIC, 377, 257, 1992
- Chengalur, J.N.: FLAGCAL: a flagging and calibration pipeline for GMRT DATA. Tech. Rep. NCRA/COM/001, NCRA-TIFR (2013)
- Devojjyoti Kansabanik, Bhaswati Bhattacharyya, Jayanta Roy, and Benjamin Stappers, The Astrophysical Journal, 920:58 (10pp), 2021 October 10
- Eggleton, P. P., The Astrophysical Journal, 268:368-369, 1983 May 1
- Foster, R. S. and Cordes, J. M., The Astrophysical Journal, 364, 123-135, 1990
- Gupta, Y., Ajithkumar, B., & Kale, H.S. et al., Current Science, 113, 707, 2017
- Hobbs, G., Edwards, R., & Manchester, R. N. 2006, MNRAS, 369, 655
- Jayanta Roy, Jayaram N. Chengalur, and Ue-Li Pen, The Astrophysical Journal, 864:160 (9pp), 2018 September 10
- Kluzniak W., Ruderman M., Shaham J., Tavani M., 1988, Nature, 334, 225
- Lorimer, D. R., Kramer, M., Handbook of Pulsar Astronomy, Cambridge observing handbooks for research astronomers, Vol. 4. Cambridge, UK: Cambridge University Press, 2004
- Lorimer D. R., SIGPROC: Pulsar Signal Processing Programs, 2011ascl.soft07016L, 2011
- Pennucci, T. T., Demorest, P. B., & Ransom, S. M. 2014, ApJ, 790, 93

- Pennucci, T. T., Demorest, P. B., Ransom, S. M. 2016, Pulse Portraiture: Pulsar timing, Astrophysics Source Code Library, ascl:1606.013
- Phinney E. S., Evans C. R., Blandford R. D., Kulkarni S. R., 1988, Nature, 333, 832
- Podsiadlowski P., 1991, Nature, 350, 136
- Prasad Jayanti, Chengalur Jayaram, Exp. Astron. 33, 157 (2012)
- Rahul Sharan, Bhaswati Bhattacharyya, Sangita Kumari, Jayanta Roy and Ankita Ghosh, Flux-density stability and temporal changes in spectra of millisecond pulsars using GMRT (in preparation)
- Roberts, M. S. E., Proceedings IAU Symposium No. 291, 2012
- Roy, J., Gupta, Y., Pen, U.L., Peterson, J.B., Kudale, S., Kodilkar, J., Exp. Astron. 28, 25, 2010
- Sangita Kumari, Bhaswati Bhattacharyya et. al, The Astrophysical Journal, 942:87 (9pp), 2023 January 10
- Sangita Kumari, Bhaswati Bhattacharyya, Rahul Sharan, Devojjyoti Kansabanik, Benjamin Stappers, and Jayanta Roy, The Astrophysical Journal, 961:155 (11pp), 2024 February 1
- Sanjay Kudale & Jayaram Chengalur, Exp Astron 44:97–112, 2017
- Scott M. Ransom, Stephen S. Eikenberry, and John Middleditch The Astronomical Journal, 124:1788–1809, 2002 September
- Shyam S. Sharma, Jayanta Roy, Bhaswati Bhattacharyya et al., The Astrophysical Journal, 936:86 (17pp), 2022 September 1
- Shyam S. Sharma, Jayanta Roy, Bhaswati Bhattacharyya, and Lina Levin, The Astrophysical Journal, 961:70 (11pp), 2024 January 20
- Suda Harshavardhan Reddy, Sanjay Kudale, Upendra Gokhale, Irappa Halagalli, Nilesh Raskar, et al., Journal of Astronomical Instrumentation, Vol. 6, No. 1 (2017) 1641011
- Taylor, J. H. 1992, RSPTA, 341, 117
- Thompson, C., Blandford, R. D., Evans, C. R., et al. The Astrophysical Journal, 422, 304, 1994

Tim Cornwell, Ed. B. Fomalont, Synthesis imaging in Radio Astronomy II, ASP conference series, Vol 180, 1999 Eds. G. B. Taylor, C. L. Carilli, and P. A. Parley

Tim J. Cornwell, Kumar Golap, and Sanjay Bhatnagar, IEEE JOURNAL OF SELECTED TOPICS IN SIGNAL PROCESSING, VOL. 2, NO. 5, OCTOBER 2008

van den Heuvel E. P. J., van Paradijs J., 1988, Nature, 334, 227